Transcription factor-promoter interactions for *PSY*/*PSYR*-mediated regulation of root growth

Authors

Jin C.-Y. Liao[1], Anne-Maarit Bågman[2,3,4], Angie J. Liu[1], Yejin Shim[1], Siobhán M. Brady[2,3,4] and Pamela C. Ronald[1,3,5,6]

Affiliations

[1]Department of Plant Pathology, University of California, Davis, CA, USA

[2]Department of Plant Biology, University of California, Davis, CA, USA

[3]Genome Center, University of California, Davis, CA, USA

[4]Howard Hughes Medical Institute (HHMI)

[5]Innovative Genomics Institute, University of California, Berkeley, CA, USA

[6]Joint Bioenergy Institute, Emeryville, CA, USA

Abstract

Precise *cis*-regulatory control of gene expression is essential for plant growth. In *Arabidopsis thaliana*, PLANT PEPTIDE CONTAINING SULFATED TYROSINE (PSY) peptides and their receptors (PSYRs) mediate growth-stress trade-offs, yet the transcriptional regulation of these genes remains poorly understood. Here, we mapped transcription factor (TF)-promoter interactions for nine *PSY* and three *PSYR* genes by combining high-throughput enhanced yeast one-hybrid screening with DNA Affinity Purification sequencing (DAP-seq) data, uncovering 1,207 interactions that reveal both shared and gene-specific regulatory relationships, defining the global TF-promoter interaction network of the *PSY*/*PSYR* pathway. Functional analysis of 25 TF mutants identified 12 regulators that significantly influence root growth, most acting as repressors. Of these, CYTOKININ RESPONSE FACTOR 10 (CRF10) emerged as a strong growth inhibitor. We identified a CRF10-binding motif in the *PSYR3* promoter using DAP-seq data and validated it using eY1H. This motif is also located in the last 3′ terminal exon of *Topoisomerase 3A* (*TOP3A*). Guided by these insights, we used CRISPR/Cas9-mediated promoter editing to delete a small region encompassing or flanking a functional TF-binding site (TFBS). Removal of this motif, or of its surrounding region, enhanced root growth, yielding variants that retained root length comparable to the *crf10* mutant. Our results suggest that the observed root growth phenotype results either from disruption of the CRF10 binding motif or from the mutation in the *TOP3A* exon.

Introduction

Plants continuously face the fundamental challenge of balancing growth and defense, two competing physiological priorities essential for survival and reproduction. Growth maximizes biomass accumulation and competitive ability, while defense mechanisms protect against pathogens and herbivores. This trade-off is tightly regulated by complex signaling networks that integrate environmental cues with internal developmental programs. Small, secreted peptides have emerged as pivotal regulators in this process. The PLANT PEPTIDE CONTAINING SULFATED TYROSINE (PSY) family and their receptors (PSYRs) form a conserved signaling module in *Arabidopsis thaliana* that modulates cell expansion, root development, and various physiological responses[1–5]. PSY peptides promote growth by stimulating cell elongation and division while interfacing with defense pathways to fine-tune resource allocation. Despite their importance, the transcriptional mechanisms controlling *PSYR* and *PSY* gene expression remain poorly defined, limiting insight into how peptide signaling adapts dynamically to environmental and developmental cues. *Cis*-regulatory elements in gene promoters serve as binding platforms for transcription factors (TFs) that orchestrate gene expression spatially and temporally, but integrating high-throughput TF-promoter interaction data into functional regulatory modules remains challenging. Precise manipulation of such *cis*-elements for trait engineering is further complicated by redundancy and incomplete functional annotation.

CRISPR/Cas-mediated promoter and *cis*-regulatory element (CRE) editing provides powerful tools to fine-tune gene expression and optimize crop traits. Approaches include multiplexed promoter targeting, CRE disruption or deletion, and promoter insertion or swapping[6]. Multiplexed CRISPR/Cas tiling screens in tomato, maize, and rice have demonstrated the potential of systematic CRE editing, although large-scale identification of functional elements remains limited[7–9]. Targeted CRE disruption has enhanced stress responses and disease resistance. In rice, editing the GT-1 element ('GAAAAA') in the *Oryza sativa RAV2* (*OsRAV2*) promoter modulated salt tolerance[10], while deletion of a TALe (Transcription Activator-Like effector)-binding element in the *SWEET11*, a sugar transporter gene, promoter improved bacterial blight resistance without affecting fertility[11–13]. Similarly, mutations in barley's *Hordeum vulgare* purple acid phosphatase a (*HvPAPhy_a*) promoter reduced phytase activity[14], and disruption of Lateral Organ Boundaries 1 (LOB1) promoter elements in citrus conferred canker resistance[15–17]. CRE editing in introns or downstream regions further expands versatility, as shown by gain-of-function *Solanum lycopersicum* WUSCHEL (*SlWUS*) alleles in tomato[7,18]. Beyond plants, CRISPR-mediated disruption of transcription factor binding sites has been demonstrated in human cells and preclinical models[19]. In crops, understanding transcriptional networks that regulate growth-defense trade-offs, where activating defense often limits growth, will be critical for engineering resilient plants with optimized productivity.

Here, we integrated high-throughput enhanced yeast one-hybrid (eY1H) screening of nine *PSY* and three *PSYR* promoters with DAP-seq data to generate a comprehensive TF-promoter interaction network comprising over 1,200 interactions. Functional validation of selected TFs through loss-of-function mutant alleles and overexpression lines identified regulators modulating *PSY/PSYR* expression and root system architecture (RSA) phenotypes. Informed by this network, we used CRISPR/Cas9-based promoter editing to

mutate a CRF10-binding motif located within the last exon of *Topoisomerase 3A*, which overlaps the *PSYR3* promoter region. These mutations led to measurable changes in *PSYR3* expression. Together, our findings establish a framework for mapping and manipulating the transcriptional regulation of the *PSY*/*PSYR* signaling pathways.

Results

Mapping the putative *PSY/PSYR* transcriptional regulatory network

To investigate transcriptional regulation underlying PSY peptide signaling, we performed enhanced yeast one-hybrid (eY1H) assays on three *PSYR* and nine *PSY* promoters using a curated *Arabidopsis* transcription factor (TF) consisting of 2,000 TFs[20]. Publicly available DAP-seq datasets[21] describe 1,207 TF-promoter interactions with ~500 TFs assessed. When integrated, these interactions revealed both shared and gene-specific regulatory relationships across the *PSY/PSYR* family, forming a comprehensive predictive transcriptional map controlling PSY and peptide transcription (Fig. 1 and Dataset S1). Network analysis further uncovered clusters of TFs potentially coordinating growth and defense responses, and several central hubs emerged as candidate regulators for functional validation. eY1H assays identify promoter-TF interactions in a chromatinized context in yeast, which can reveal potential regulatory relationships but may include false positives and negatives. Published studies have shown that a subset of eY1H-identified interactions is supported by *in planta* validation, such as ChIP or genetic analysis[22,23]. In contrast, DAP-seq profiles interactions between individual TFs and DNA sequences *in vitro*, providing high-resolution information on potential binding sites but not direct evidence of *in vivo* occupancy[21]. Integration of both datasets revealed limited overlap between the two datasets. Specifically, three TFs were identified to interact with the *PSYR1* promoter, eight for *PSYR2*, six for *PSYR3*, sixteen for *PSY1*, four for *PSY2*, two for *PSY3*, seven for *PSY4*, one for *PSY5-8*, and three for *PSY9* (Fig. S1 and Dataset S2). Together, these shared interactions highlight a small but robust set of candidate regulators supported by both approaches[24].

To investigate how these regulatory interactions are reflected *in planta*, we examined gene expression patterns across tissues and cell types. Analyses of publicly available RNA-seq datasets[25] defined the expression profiles of *PSYR* and *PSY* genes throughout Arabidopsis organs. All three *PSYR*s were broadly expressed, with *PSYR1* enriched in shoots and *PSYR3* in roots (Fig. S2). Among the peptides, *PSY1* was the most abundant and widely expressed, whereas *PSY7* showed minimal expression. *PSY4* was predominantly localized to roots, and *PSY9* was mainly expressed in seeds (Fig. S2). Single-cell data from the Plant sc-Atlas[26] further revealed cell-type specificity. *PSY3* and *PSY4* co-localized in root cell types, suggesting overlapping functions, while *PSY6* and *PSY8* displayed distinct but complementary root-specific patterns (Fig. S3). Together, these findings highlight potential links between spatial regulation, receptor-ligand interplay, and root system architecture (RSA).

Network-guided selection and screening of TFs for promoter editing

To systematically prioritize TFs for functional analysis, we combined whole-promoter interaction assays (eY1H) with DAP-seq data, identifying 40 high-confidence candidates. From these, 12 TFs with available homozygous mutant lines and an additional 10 TFs detected only by DAP-seq (represented by 13 independent homozygous alleles) were selected for phenotypic analysis (Dataset S2, S3, Table S2). Using these prioritized TFs, we then mapped their respective transcription factor binding sites (TFBS) across all three *PSYR* and nine *PSY* promoters to identify precise promoter regions for targeted editing. We focused on root system architecture (RSA) as a readout, given its responsiveness to genetic and environmental cues and the availability of high-throughput phenotyping tools. We then developed a workflow integrating TFBS mapping with functional assays to pinpoint regulatory regions suitable for CRISPR-based promoter editing (Fig. 2a). Although a root-specific DAP-seq dataset would be ideal, it is not currently available, underscoring the importance of combining multiple data sources for candidate prioritization.

While *PSY1* overexpression and the *psyr1,2,3* triple mutant have been reported to alter primary root length[1–3,27], other RSA phenotypes in these lines, as well as in single *PSY* or *PSYR* mutants, remain unknown. Given the root cell type expression patterns of *PSY/PSYR* genes, we focused on phenotypic analysis of mutants for the 12 TFs identified by both eY1H and DAP-seq. Knockouts were first validated by PCR genotyping and qRT-PCR (Fig. S5). Single mutant alleles of ten TF mutants (*crf10*, *tga2 tga5*, *wrky8-1*, *myb77-2*, *myb73-1*, *hb34*, *myb70-2*, *at3g42860*, *abi5-10*, *wrky14*) displayed increased primary root length, while two mutants (*rap2.11*, *atrav1.1*) showed no change (Fig. 2b-d). In addition to these 12 TFs, we also analyzed DAP-seq-only candidates for phenotypic effects, as homozygous mutant lines were available and they could reveal additional regulators of root growth not detected by eY1H. Among the DAP-seq-only TFs, six alleles of four TFs (*wrky22-1, wrky22-2, wrky22-3, anac087-2, erf11, aif*) displayed increased root length, one allele (*ein3-1*) showed decreased root length, and seven alleles (*hca2, pear2, myb3r4-3, tga10, ntl4-1, erf4-1, ntl8-1*) exhibited no change (Fig. S6). Many of these alleles had been studied previously, but root phenotypes were largely unreported or poorly described, with *myb70-2* as the only clearly documented case[28], showing a longer primary root consistent with our observations. Overall, 26 mutants of 24 TFs exhibited significant changes in root growth compared with wild-type plants, 16 of which displayed increased biomass and enhanced root growth, suggesting that multiple TFs negatively regulate growth to fine-tune developmental outcomes (Data S3). We tested the less-characterized candidate CRF10 and found that overexpression caused stunted growth, whereas the *crf10* knockout displayed enhanced growth compared with wild type (Fig. 2 b-d and Fig. S7). Collectively, these results suggest that the identified TFs contribute to root growth regulation, highlighting the potential of promoter-targeted approaches to modulate RSA phenotypes.

Transcript levels in shoots and roots of selected TF knockout lines

To assess whether candidate TFs act as activators or repressors of *PSY/PSYR* transcription and whether their regulation is organ-specific, we measured transcript levels in shoots and roots of selected TF knockout lines using quantitative RT-PCR (qRT-PCR)

(Fig. 3). The same homozygous knockout lines that were genotyped and phenotypically validated in Fig. 2c were used for these expression assays, ensuring that transcriptional differences could be directly linked to previously observed RSA phenotypes. We focused on the three *PSYR* and three *PSY* (*PSY1*, *PSY2*, *PSY4*) promoters with the highest number of candidate TF interactions identified by eY1H, and for which binding sites were also detected in DAP-seq (Fig. 3). Shoot and root organs from these validated lines were collected separately to capture potential organ-specific regulation. qRT-PCR analyses revealed consistent significant differences in *PSYR* and *PSY* expression (Fig. 3), directly connecting TF-promoter interactions to transcriptional outputs.

Among the analyzed mutants, *myb73*, *myb70*, and *crf10* showed significantly altered expression of *PSY/PSYR* target genes, with distinct patterns of activation and repression. MYB70 bound the promoters of both *PSYR1* and *PSYR2* and repressed *PSYR2* transcription, as loss of MYB70 led to a ~1.9-fold increase relative to WT (p = 0.0236) in the shoot, whereas MYB73 bound the *PSYR1* promoter and activated *PSYR1* transcription, as loss of MYB73 reduced expression to ~0.14-fold relative to WT (p = 0.0064) in the root. CRF10 bound the *PSYR3* promoter and activated transcription in both organs, as loss of CRF10 reduced expression to ~0.64-fold relative to WT in the shoot (p = 0.0383) and ~0.53-fold relative to WT in the root (p = 0.0012). Several mutants of additional TFs, including TGA5, WRKY8, ABI5, and RAV2.11, were tested for effects on *PSY*/*PSYR* gene expression (Fig. 3 and Data S4), but their precise regulatory roles remain unclear and will require further analysis, including more biological replicates and other mutant alleles. The transcriptional changes observed in *myb70*, *myb73*, and *crf10* are consistent with direct TF-mediated regulation, and the magnitude and organ specificity of these changes corresponded with the root phenotypes of the respective knockout lines, suggesting that these TFs may contribute to fine-tuning *PSY*/*PSYR* signaling.

Mutation of the CRF10 binding motif in the *PSYR3* promoter/*TOP3A* final exon affects root growth in genome-edited lines

To test whether disruption of transcription factor binding sites could modulate gene expression and plant growth, we implemented a CRISPR/Cas9-based promoter editing strategy. Candidate motifs within *the PSYR3* promoter were targeted, which overlap with the last exon of the *Topoisomerase 3A* (*TOP3A*) coding region. A putative CRF10 binding motif ('CGGCGG') was identified in the *PSYR3* promoter using DAP-seq data and validated by eY1H. CRF10 is a member of the APETALA2 (AP2)/ETHYLENE RESPONSE FACTOR (ERF) transcription factor family, which regulates hormone signaling, stress responses, and development[29]. Although the *Arabidopsis* CRF family contains 12 members, CRF10 remains largely uncharacterized. In Col-0 plants, *CRF10* was expressed ubiquitously, with the highest expression in embryos (Fig. S4). In our screening (Fig. 2), *crf10* mutants exhibited longer primary roots and overall enhanced root system architecture (RSA), characterized by increased lateral root number and length as well as greater total root length (Fig. 2b-d). Overexpression of *CRF10* in wild-type Col-0, in two independent lines, caused growth inhibition, confirming that *CRF10* functions as a negative regulator of growth (Fig. S7).

To test whether CRF10 binding influences *PSYR3* expression, we generated CRISPR-edited lines targeting the CRF10 motif in the *PSYR3* promoter/*TOP3A* final exon. Two guide RNAs were designed to target both the primary TFBS and adjacent sequences (Fig. 4a). Sequencing of independent lines revealed two distinct alleles. R3pro_Var1 carries a 31 bp deletion immediately adjacent to the DAP-seq-validated CRF10 binding motif, leaving the consensus sequence intact, whereas R3pro_Var2 carries a 27 bp deletion that removes the motif entirely. T2 homozygous lines were used for phenotyping and expression assays. Notably, R3pro_Var1 and R3pro_Var2 alleles are also present in the last 3′ terminal exon of *Topoisomerase 3A* (*TOP3A*), raising the possibility that the phenotypes observed in the promoter-edited variants may be due to the TOP3A mutation (Fig. 4a). The *top3a-1* mutant carries a T-DNA insertion that abolishes mRNA spanning the insertion site, resulting in a knockout allele with severe developmental defects or early lethality[31]. *top3a-2* carries a T-DNA insertion upstream in the gene, producing a hypomorphic allele that is viable but completely sterile, with milder growth abnormalities such as dwarfing and organ curling[30,31]. In the absence of available phenotypes for mutations in the last exon of *TOP3A*, it is unknown whether such mutations confer the same phenotype observed in our study.

Phenotypic analysis revealed that promoter-edited plants exhibited altered primary root length compared with wild type, with phenotypes comparable in magnitude to *psyr3-1* and *crf10* knockout mutants (Fig. 4c). Lateral root number remained unchanged (Fig. 4d), but total lateral root length per plant increased (Fig. 4e), resulting in increased total and average lateral root length relative to WT, *psyr3-1*, and *crf10* (Fig. 4f). Both edited alleles showed a mild reduction in *PSYR3* transcript abundance in shoots and roots, with R3pro_Var1 and R3pro_Var2 exhibiting ~0.78- and ~0.56-fold expression relative to wild-type controls (Fig. 4g). Although these decreases were not statistically significant in R3pro_Var1 (shoot: $P = 0.3754$; root: $P = 0.0626$) or in the root of R3pro_Var2 ($P = 0.0719$), the shoot of R3pro_Var2 showed a significant reduction ($P = 0.0053$), with the CRF10 consensus motif removed. This trend suggests that CRF10 consensus motif and sequences adjacent to the motif may contribute to transcriptional regulation, although effects from the linked *TOP3A* mutation cannot be excluded.

Discussion

Our work demonstrates the utility of network-guided promoter analysis to identify putative TF binding sites. We observed altered root growth phenotypes in plants where the CRF10 binding motif itself was deleted, and when nearby promoter regions were perturbed. Notably, the CRF10 binding motif we analyzed is also located in the last 3′ terminal exon of *Topoisomerase 3A* (*TOP3A*). Thus, we cannot rule out the possibility that the observed root growth phenotypes are also due to the mutated TOP3A.

TF-promoter interaction analysis of the *PSY-PSYR* signaling pathway provides a framework for future precise, context-aware trait modulation. By leveraging functional *cis* elements identified from regulatory networks, edits can be tailored for spatially precise regulation at the organ, tissue, or even cell level, in addition to being environment-

254 responsive, thereby enhancing trait specificity while minimizing unintended systemic
255 effects. This capability is particularly valuable for complex traits influenced by multiple
256 environmental and developmental cues, where traditional knockout approaches may
257 produce broad pleiotropic effects. Future work will be directed at genome editing of
258 experimentally validated TF binding site motifs with the aim of optimizing traits while
259 preserving overall plant fitness.

260 Although tiling-deletion-based screens have enabled systematic functional interrogation
261 of regulatory regions, they are labor-intensive, time-consuming, and often less predictive,
262 particularly when applied across multiple genes. Moreover, because these strategies rely
263 on scanning promoter regions through serial deletion or mutagenesis, they tend to reveal
264 functional elements retrospectively rather than enabling targeted modulation. In contrast,
265 our gene regulatory network-guided strategy enables identification of putative functional
266 *cis*-regulatory elements. This hypothesis-driven approach sets up a framework for future
267 fine-tuning of gene expression. By narrowing the range of potential target sites, network-
268 guided predictions allow the researcher to design genome edits that can enhance both
269 predictability and efficiency. Although promoter insertions or swaps remain technically
270 challenging, successful examples, such as the insertion of the *GOS2* promoter upstream
271 of *ARGOS8* in maize to enhance expression and improve drought tolerance[32],
272 demonstrate the potential for context-aware regulatory engineering and create
273 opportunities for synthetic promoter applications by replacing native promoters.

274 Promoter editing in Arabidopsis remains largely unexplored, yet the species offers rich
275 genomic and regulatory resources, including well-characterized gene regulatory
276 networks, TFBS maps, and promoter motifs. Comparative analyses between Arabidopsis
277 and crop species will be essential to translate these insights to agricultural contexts. While
278 gene regulatory networks are extensively mapped in Arabidopsis, coverage in major
279 crops remains limited. Systematic comparisons of TFBSs, promoter architectures, and
280 regulatory modules can identify conserved elements, enabling rational design of network-
281 guided promoter edits in Arabidopsis and crop species. Future studies will explore
282 whether promoter edits of putative TFBSs in the *PSY*/*PSYR* promoters affect RSA and
283 pathogen resistance. Integrating ATAC-seq or other chromatin profiling approaches in
284 edited lines will provide deeper insight into the epigenomic consequences of TFBS-level
285 perturbations and help refine predictive models of *cis*-regulatory engineering.

286

287 **Methods**

288 **Promoter cloning for eY1H.**

289 *PSYR* and *PSY* gene promoters previously tested in Ogawa-Ohnishi et al.[1] were cloned
290 using the method described by Gaudinier et al.[22,33]. Promoters were amplified by PCR
291 from *Arabidopsis thaliana* Col-0 genomic DNA using Phusion High-Fidelity DNA
292 Polymerase (NEB). The amplified promoter fragments were first cloned into the pENTR
293 5'TOPO vector using the pENTR 5'TOPO kit (Invitrogen) and fully sequenced.
294 Subsequently, promoters were recombined with the Gateway LR reaction into both pMW2
295 and pMW3[41] Gateway destination vectors (designed for yeast expression and containing
296 respectively *HIS3* or *LacZ* reporter genes) using LR Clonase™ II (Invitrogen). The

resulting constructs were sent to Azenta Life Sciences (South Plainfield, NJ, USA; formerly GeneWiz) for whole plasmid sequencing using the Plasmid-EZ nanopore-based sequencing method.

Enhanced Yeast One Hybrid (eY1H) Assay.

Assays were performed according to Gaudinier et al.[22,33]. *PSYR* and *PSY* promoter – pMW2/pMW3 reporter constructs were transformed into yeast strain YM4271. Resulting yeast colonies were screened for autoactivation for both histidine biosynthesis and lacZ activity, and the construct presence within the yeast genome was confirmed by PCR-based genotyping. The resulting bait yeast strains were screened against a complete collection of 2000 Arabidopsis transcription factors[34] in a mating-based assay, and positive interactions were identified for both histidine and lacZ activity compared to a negative control pDESTAD-2μ. An interaction was recorded as successful if there was activation of either HIS or lacZ. The eY1H Yeast One-Hybrid screening was carried out by the Yeast One-Hybrid Services Core at the UC Davis Genome Center, at the University of California, Davis. The table with all the results can be found at https://github.com/jcyliao/Liao2025.

Network construction.

Networks were made using Cytoscape v.3.10.2[35]. All cytoscape network files can be found at https://github.com/jcyliao/Liao2025.

DAP-seq data comparison and mutant lines selection.

DAP-seq TF binding data generated by O'Malley et al.[21] were used to identify direct TF-promoter interactions. DAP-seq target genes (fraction of reads in peaks [FRiP] ≥ 5%) for 529 TFs were downloaded from the Plant Cistrome Database. TFs binding to each individual *PSY/PSYR* promoter were extracted from the DAP-seq data (Dataset S1). A Python script was then used to compare the TF lists for each promoter from eY1H and DAP-seq experiments, generating lists of overlapping TFs identified by both assays (Dataset S2).

From these comparisons, 40 overlapping TFs and ~20 TFs identified only in DAP-seq were selected based on the availability of loss-of-function mutants. Mutant lines previously used in published studies were prioritized (Table S2).

Expression analysis of *PSY/PSYR* genes and their regulatory TFs.

Expression patterns of *PSYR* and *PSY* genes, along with their selected potential regulatory transcription factors (TFs) identified from eY1H and DAP-seq, were analyzed using publicly available datasets. Bulk RNA-seq datasets were collected to examine gene expression across different tissues and developmental stages. Single-cell RNA-seq

336 datasets, including root cell type-specific profiles from the Plant sc-Atlas database[26], were
337 used to assess cell type-specific expression. Comparative analyses were performed to
338 identify co-expression patterns and potential tissue- or cell type-specific regulatory
339 relationships.

340

341 **Plant materials and growth conditions.**

342 All transgenic lines were generated in the *Arabidopsis thaliana* Col-0 accession, except
343 for *abi5-1*, which was in the Ws-2 background. Loss-of-function TF mutants were obtained
344 from the Arabidopsis Biological Resource Center (ABRC) at Ohio State University. All
345 mutant lines, including those carrying T-DNA insertions, fast neutron-induced mutations,
346 or EMS-induced mutations, were genotyped to confirm homozygosity. Quantitative RT-
347 PCR (qRT-PCR) was performed to verify transcript-level alterations (Fig. S5 and Data
348 S4). The primers used for genotyping and qRT-PCR, along with accession numbers and
349 additional details on the analyzed mutant lines, are provided in Supplementary Table 2.
350 Plants were grown under a 16-hour light/8-hour dark photoperiod for propagation.

351

352 **Generation of TF overexpressing transgenic plants.**

353 The coding sequences for each TF used in this study were obtained from the TF ENTR
354 clone collection[34] and subsequently cloned into the N-GFP tag pGWB506 (Addgene
355 #74848) destination vector using LR Clonase™ II (Invitrogen) for overexpression in
356 plants. The resulting GFP-TF constructs, driven by the 35S promoter, were introduced
357 into *Agrobacterium tumefaciens* strain GV3101 and used to transform *A. thaliana* (Col-0)
358 via the floral dip method[36]. At least ten independent transgenic lines were selected on ½
359 MS solid medium supplemented with 25 mg/L hygromycin. Transgene expression was
360 assessed through GFP fluorescence microscopy and PCR. For each genotype, two to
361 three independent T3 homozygous plants were used for subsequent phenotypic
362 analyses. The primers used for genotyping and accession numbers, and additional details
363 on the constructs, are provided in Supplementary Table 1.

364

365 **Plant phenotype analysis of the TF mutants.**

366 Homozygous TF loss-of-function mutants, TF overexpression T3 plants, and the wild-type
367 (WT) controls were sterilized with 25% (v/v) bleach for 20 min, followed by 5 washes with
368 sterile Milli-Q water. Sterilized seeds were plated on ½ MS medium supplemented with
369 1% sucrose and 0.6% Gelzan, then stratified at 4°C for 2-3 days before being transferred
370 to a growth chamber under long-day (LD) conditions (16 h light/8 h dark) with 50-60%
371 humidity at 22°C. Mutant lines and wild-type controls were arranged in a randomized
372 block design within the growth chamber. Plate images were scanned at 10 days post-
373 germination (10 dpg) using an Epson Expression 12000XL scanner at 300 dpi resolution.
374 Root traits were measured from the scanned images, with at least 20 plants per genotype
375 included in each experimental replicate. The experiment was repeated independently
376 three times. For root trait measurements, RootNav 1.0[37] was used for image analysis and

377 data extraction. Traits measured included primary root length (PRL), lateral root number
378 (LR) and lateral root length (LRL). Composite traits were analyzed, including total root
379 length (TRL = PRL + LRL), average lateral root length (ALRL = LRL/LR), lateral root
380 density (LRD = LR/PRL), and the percentage of LRL contributing to TRL (LRL/TRL).
381 Variation across these mutants relative to WT was assessed using one-way ANOVA for
382 all RSA traits. Statistical analyses were performed in Python, with significance determined
383 by Tukey's HSD test.

384

385 **RNA extraction and quantitative PCR.**

386 The whole root and shoot parts of 10-day-old seedlings were collected separately. For
387 one shoot sample, shoots from 10 seedlings grown on the same plate were pooled
388 together. For one root sample, roots from 30 seedlings grown on the same experiment
389 were pooled together. Three independent replicates per genotype were collected. Total
390 RNA was extracted using TRIzol reagent (Invitrogen) for TF mutant screening
391 experiments and using the RNeasy Plant Mini Kit (QIAGEN) for promoter-edited line
392 experiments, following the manufacturer's instructions. Genomic DNA contamination
393 was removed by RNase-free DNase treatment during RNA extraction, according to the
394 manufacturer's protocols. First-strand cDNA was synthesized using the SuperScript™
395 III First-Strand Synthesis System for RT-PCR (Invitrogen) following the manufacturer's
396 instructions. Quantitative real-time PCR (qRT-PCR) was performed using iTaq™
397 Universal SYBR Green Supermix (Bio-Rad) on a Bio-Rad CFX96 Real-Time System
398 coupled with a C1000 Thermal Cycler (Bio-Rad) under the following conditions: initial
399 denaturation at 95°C for 30 s, followed by 39 cycles of PCR (denaturation at 95°C for 5
400 s, annealing at 60°C for 30 s, and extension at 72°C for 20 s). Relative gene expression
401 was determined using the $2^{-\Delta\Delta CT}$ method, with ACTIN2 as the endogenous control. The
402 primers used for qRT-PCR are provided in Supplementary Table 1.
403

404 **Generation of CRISPR/Cas9 promoter editing of CRF10 binding site and plant**
405 **screening**

406 Promoter regions containing characterized TFBSs were selected based on TF-promoter
407 interaction mapping and mutant phenotypes. Guide RNAs (gRNAs) were designed to
408 flank these sites, and corresponding CRISPR/Cas9 constructs were generated using
409 standard cloning protocols.

410 For the generation of pJL-AtU6.26-gPSYR3-S1S2 entry clone, an EcoRI-AtU6-26
411 promoter-partial pQZ435–BsaI gBlock was synthesized via the IDT gBlock service.
412 gRNAs were designed using CHOPCHOP[38], and PTG assembly into pQZ435, with the
413 OsU3 promoter removed, was performed following Xie et al.[39] with minor modifications.
414 The entry clone was transferred into the pRU294 destination vector via Gateway LR
415 recombination, following the manufacturer's instructions, and the resulting construct was
416 transformed into *Agrobacterium tumefaciens* GV3101 for plant transformation. Constructs
417 were transformed into *Arabidopsis thaliana* via Agrobacterium-mediated floral dipping.
418 Rapid screening of Cas9-containing and Cas9-free lines in both T1 and T2 generations
419 was conducted using a seed coat fluorescence marker[40]. Transgenic plants were

confirmed by PCR and Sanger sequencing to confirm precise edits disrupting TFBSs. Successfully edited lines were propagated for subsequent phenotypic and gene expression analyses.

Figure preparation and statistical analysis

Python was used for statistical analyses and to generate plots. Figures were assembled in Microsoft PowerPoint. Some illustrations in the workflow (Fig. 2a) were created using BioRender.

Data availability

All supplementary datasets, Cytoscape files, and Python code are available at https://github.com/jcyliao/Liao2025.

Use of AI

ChatGPT (OpenAI) assisted only with improving the phrasing of some paragraphs and did not generate any new content.

Acknowledgements

We thank Bhanu Upadhyayula, Kai Deshpande, and Maya Ziebarth for assistance with organizing genetic materials and performing genotyping experiments. We are also grateful to Valley Stewart for guidance and mentoring, and to Qiong Zhang for providing the pQZ435 vector and the modified PTG cloning protocol. This work was supported by the Chan Zuckerberg Initiative and NIH MIRA grant #R35 GM148173 to P.C.R. We thank Idan Efroni for critical reading of the manuscript and for helpful suggestions.

Author contributions

J.C.-Y.L. conceived the project, designed the experiments, and conducted most of the experiments and all data analysis. A.B. and the Yeast One-Hybrid (Y1H) Services Core conducted all eY1H screenings. J.C.-Y.L. and A.J.L. prepared samples for the gene expression assays. A.J.L. performed most of the root phenotyping raw data acquisition and, together with Y.S., carried out qRT-PCR measurements. Both A.J.L. and Y.S. participated in mutant screening. P.C.R. supervised the work and provided funding and resources. J.C.-Y.L. wrote the manuscript. P.C.R. and J.C.-Y.L. revised the MS with input from S.M.B.

References

456 1. Ogawa-Ohnishi, M. *et al.* Peptide ligand-mediated trade-off between plant growth and
457 stress response. *Science* **378**, 175–180 (2022).
458 2. Wang, Y., Chen, W., Ou, Y., Zhu, Y. & Li, J. Arabidopsis ROOT ELONGATION
459 RECEPTOR KINASES negatively regulate root growth putatively via altering cell wall
460 remodeling gene expression. *J Integr Plant Biol* **64**, 1502–1513 (2022).
461 3. Ercoli, M. F., Shigenaga, A. M., Araujo, A. T. de, Jain, R. & Ronald, P. C. Tyrosine-
462 sulfated peptide hormone induces flavonol biosynthesis to control elongation and
463 differentiation in Arabidopsis primary root. 2024.02.02.578681 Preprint at
464 https://doi.org/10.1101/2024.02.02.578681 (2024).
465 4. Yimer, H. Z. *et al.* Root-knot nematodes produce functional mimics of tyrosine-
466 sulfated plant peptides. *Proceedings of the National Academy of Sciences* **120**,
467 e2304612120 (2023).
468 5. Ercoli, M. F. *et al.* Plant immunity: Rice XA21-mediated resistance to bacterial
469 infection. *Proc. Natl. Acad. Sci. U. S. A.* **119**, (2022).
470 6. Li, Q., Sapkota, M. & van der Knaap, E. Perspectives of CRISPR/Cas-mediated cis-
471 engineering in horticulture: unlocking the neglected potential for crop improvement.
472 *Hortic Res* **7**, 1–11 (2020).
473 7. Rodríguez-Leal, D., Lemmon, Z. H., Man, J., Bartlett, M. E. & Lippman, Z. B.
474 Engineering Quantitative Trait Variation for Crop Improvement by Genome Editing.
475 *Cell* **171**, 470-480.e8 (2017).
476 8. Liu, L. *et al.* Enhancing grain-yield-related traits by CRISPR–Cas9 promoter editing of
477 maize CLE genes. *Nat. Plants* **7**, 287–294 (2021).

478 9. Song, X. *et al.* Targeting a gene regulatory element enhances rice grain yield by
479 decoupling panicle number and size. *Nat Biotechnol* **40**, 1403–1411 (2022).
480 10. Duan, Y.-B. *et al.* Identification of a regulatory element responsible for salt induction
481 of rice OsRAV2 through ex situ and in situ promoter analysis. *Plant Mol Biol* **90**, 49–
482 62 (2016).
483 11. Xu, Z. *et al.* Engineering Broad-Spectrum Bacterial Blight Resistance by
484 Simultaneously Disrupting Variable TALE-Binding Elements of Multiple Susceptibility
485 Genes in Rice. *Molecular Plant* **12**, 1434–1446 (2019).
486 12. Li, C. *et al.* A new rice breeding method: CRISPR/Cas9 system editing of the Xa13
487 promoter to cultivate transgene-free bacterial blight-resistant rice. *Plant*
488 *Biotechnology Journal* **18**, 313–315 (2020).
489 13. Oliva, R. *et al.* Broad-spectrum resistance to bacterial blight in rice using genome
490 editing. *Nat Biotechnol* **37**, 1344–1350 (2019).
491 14. Holme, I. B. *et al.* Evaluation of the mature grain phytase candidate HvPAPhy_a
492 gene in barley (Hordeum vulgare L.) using CRISPR/Cas9 and TALENs. *Plant Mol*
493 *Biol* **95**, 111–121 (2017).
494 15. Jia, H., Orbović, V. & Wang, N. CRISPR-LbCas12a-mediated modification of citrus.
495 *Plant Biotechnology Journal* **17**, 1928–1937 (2019).
496 16. Jia, H., Orbovic, V., Jones, J. B. & Wang, N. Modification of the PthA4 effector
497 binding elements in Type I CsLOB1 promoter using Cas9/sgRNA to produce
498 transgenic Duncan grapefruit alleviating XccΔpthA4:dCsLOB1.3 infection. *Plant*
499 *Biotechnology Journal* **14**, 1291–1301 (2016).

500 17. Peng, A. *et al.* Engineering canker-resistant plants through CRISPR/Cas9-targeted
501 editing of the susceptibility gene CsLOB1 promoter in citrus. *Plant Biotechnol. J.* **15**,
502 1509–1519 (2017).
503 18. Li, T. *et al.* Domestication of wild tomato is accelerated by genome editing. *Nat*
504 *Biotechnol* **36**, 1160–1163 (2018).
505 19. Li, X. *et al.* Programmable base editing of mutated TERT promoter inhibits brain
506 tumour growth. *Nat Cell Biol* **22**, 282–288 (2020).
507 20. Tang, M. *et al.* A genome-scale TF–DNA interaction network of transcriptional
508 regulation of Arabidopsis primary and specialized metabolism. *Molecular Systems*
509 *Biology* **17**, e10625 (2021).
510 21. O'Malley, R. C. *et al.* Cistrome and Epicistrome Features Shape the Regulatory
511 DNA Landscape. *Cell* **165**, 1280–1292 (2016).
512 22. Gaudinier, A. *et al.* Enhanced Y1H assays for Arabidopsis. *Nat Methods* **8**, 1053–
513 1055 (2011).
514 23. Gaudinier, A. *et al.* Transcriptional regulation of nitrogen-associated metabolism and
515 growth. *Nature* **563**, 259–264 (2018).
516 24. Sparks, E. E. *et al.* Establishment of Expression in the SHORTROOT-
517 SCARECROW Transcriptional Cascade through Opposing Activities of Both
518 Activators and Repressors. *Developmental Cell* **39**, 585–596 (2016).
519 25. Zhang, H. *et al.* A Comprehensive Online Database for Exploring ~20,000 Public
520 Arabidopsis RNA-Seq Libraries. *Molecular Plant* **13**, 1231–1233 (2020).
521 26. Wendrich, J. R. *et al.* Vascular transcription factors guide plant epidermal responses
522 to limiting phosphate conditions. *Science* **370**, eaay4970 (2020).

523 27. Amano, Y., Tsubouchi, H., Shinohara, H., Ogawa, M. & Matsubayashi, Y. Tyrosine-
524 sulfated glycopeptide involved in cellular proliferation and expansion in Arabidopsis.
525 *Proc Natl Acad Sci U S A* **104**, 18333–18338 (2007).
526 28. Wan, J. *et al.* MYB70 modulates seed germination and root system development in
527 Arabidopsis. *iScience* **24**, 103228 (2021).
528 29. Rashotte, A. M. *et al.* A subset of Arabidopsis AP2 transcription factors mediates
529 cytokinin responses in concert with a two-component pathway. *Proceedings of the*
530 *National Academy of Sciences* **103**, 11081–11085 (2006).
531 30. Hartung, F., Suer, S., Knoll, A., Wurz-Wildersinn, R. & Puchta, H. Topoisomerase
532 3α and RMI1 Suppress Somatic Crossovers and Are Essential for Resolution of
533 Meiotic Recombination Intermediates in Arabidopsis thaliana. *PLOS Genetics* **4**,
534 e1000285 (2008).
535 31. Hartung, F., Suer, S. & Puchta, H. Two closely related RecQ helicases have
536 antagonistic roles in homologous recombination and DNA repair in Arabidopsis
537 thaliana. *Proceedings of the National Academy of Sciences* **104**, 18836–18841
538 (2007).
539 32. Shi, J. *et al.* ARGOS8 variants generated by CRISPR-Cas9 improve maize grain
540 yield under field drought stress conditions. *Plant Biotechnology Journal* **15**, 207–216
541 (2017).
542 33. Gaudinier, A., Tang, M., Bågman, A.-M. & Brady, S. M. Identification of Protein–
543 DNA Interactions Using Enhanced Yeast One-Hybrid Assays and a Semiautomated
544 Approach. in *Plant Genomics: Methods and Protocols* (ed. Busch, W.) 187–215
545 (Springer, New York, NY, 2017). doi:10.1007/978-1-4939-7003-2_13.

546 34. Pruneda-Paz, J. L. *et al.* A Genome-Scale Resource for the Functional
547 Characterization of Arabidopsis Transcription Factors. *Cell Reports* **8**, 622–632
548 (2014).
549 35. Shannon, P. *et al.* Cytoscape: A Software Environment for Integrated Models of
550 Biomolecular Interaction Networks. *Genome Res.* **13**, 2498–2504 (2003).
551 36. Clough, S. J. & Bent, A. F. Floral dip: a simplified method for Agrobacterium-
552 mediated transformation of Arabidopsis thaliana. *Plant J.* **16**, 735–43 (1998).
553 37. Pound, M. P. *et al.* RootNav: Navigating Images of Complex Root Architectures.
554 *Plant Physiol* **162**, 1802–1814 (2013).
555 38. Labun, K. *et al.* CHOPCHOP v3: expanding the CRISPR web toolbox beyond
556 genome editing. *Nucleic Acids Research* **47**, W171–W174 (2019).
557 39. Xie, K., Minkenberg, B. & Yang, Y. Boosting CRISPR/Cas9 multiplex editing
558 capability with the endogenous tRNA-processing system. *Proceedings of the National*
559 *Academy of Sciences* **112**, 3570–3575 (2015).
560 40. Ursache, R., Fujita, S., Dénervaud Tendon, V. & Geldner, N. Combined fluorescent
561 seed selection and multiplex CRISPR/Cas9 assembly for fast generation of multiple
562 Arabidopsis mutants. *Plant Methods* **17**, 111 (2021).
563 41. Deplancke, B., Vermeirssen, V., Arda, H. E., Martinez, N. J. & Walhout, A. J. M.
564 Gateway-Compatible Yeast One-Hybrid Screens. *Cold Spring Harb Protoc* **2006**,
565 pdb.prot4590 (2006).
566
567
568

Figures

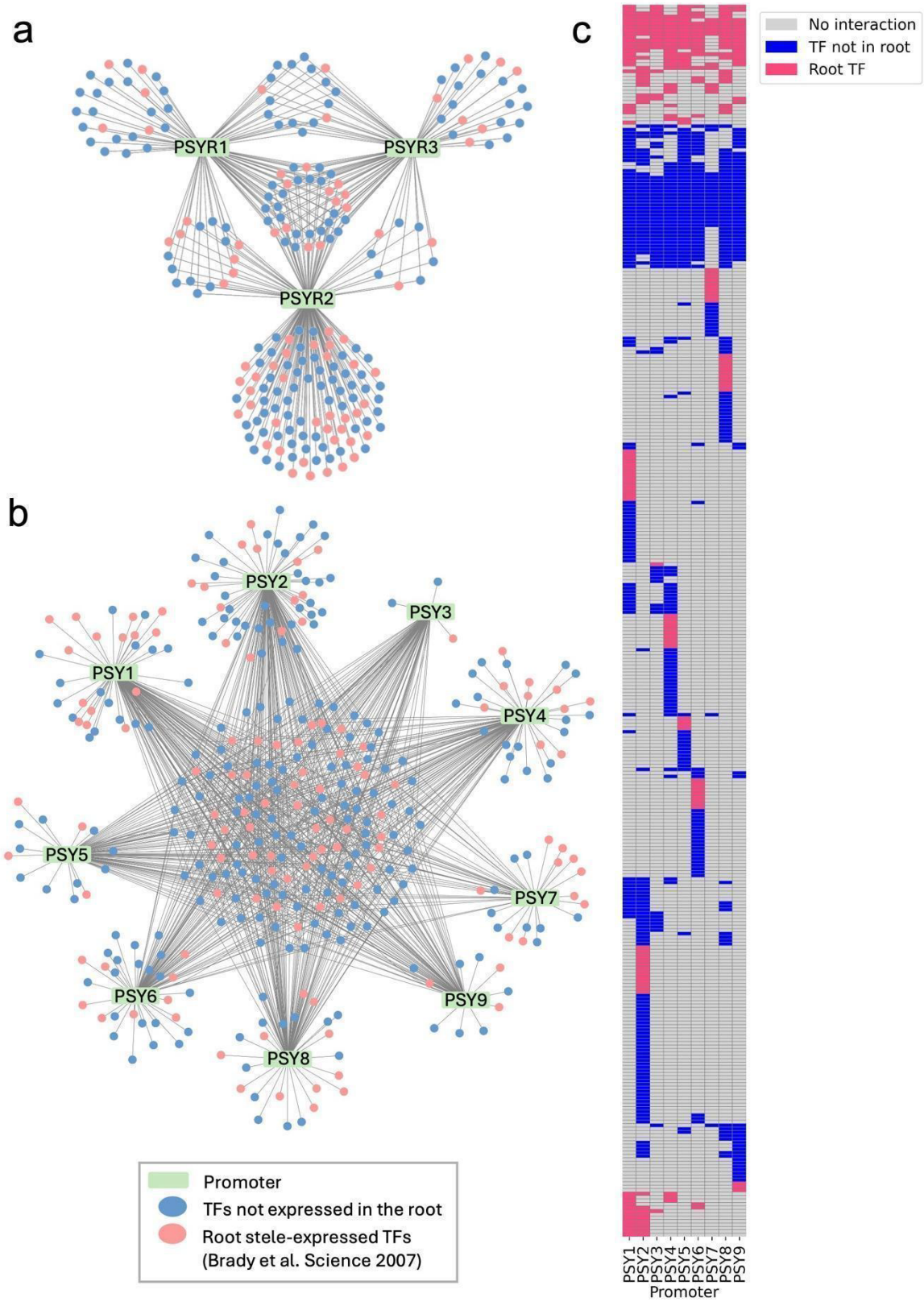

572

573 **Fig. 1. TF-*PSY/PSYR* promoter interaction network.**

574 **a.** TF-promoter interactions involved in PSY perception, identified by eY1H (*PSYR1-*
575 *PSYR3*, 3 promoters).
576 **b.** TF-promoter interactions involved in PSY peptide transcription, identified by eY1H
577 (*PSY1-PSY9*, 9 promoters). Rectangles represent promoters; small circles represent
578 TFs. Pink circles indicate root-expressed TFs (Brady et al., 2007), and blue circles
579 indicate TFs outside the root stele-expressed set.
580 **c.** Heatmap of TF-promoter interactions for PSY peptide transcription identified by
581 eY1H, with shared TFs clustered. Coloring follows panel b: pink = root-expressed TFs
582 (Brady et al., 2007), blue = TFs outside the root stele-expressed set.

583

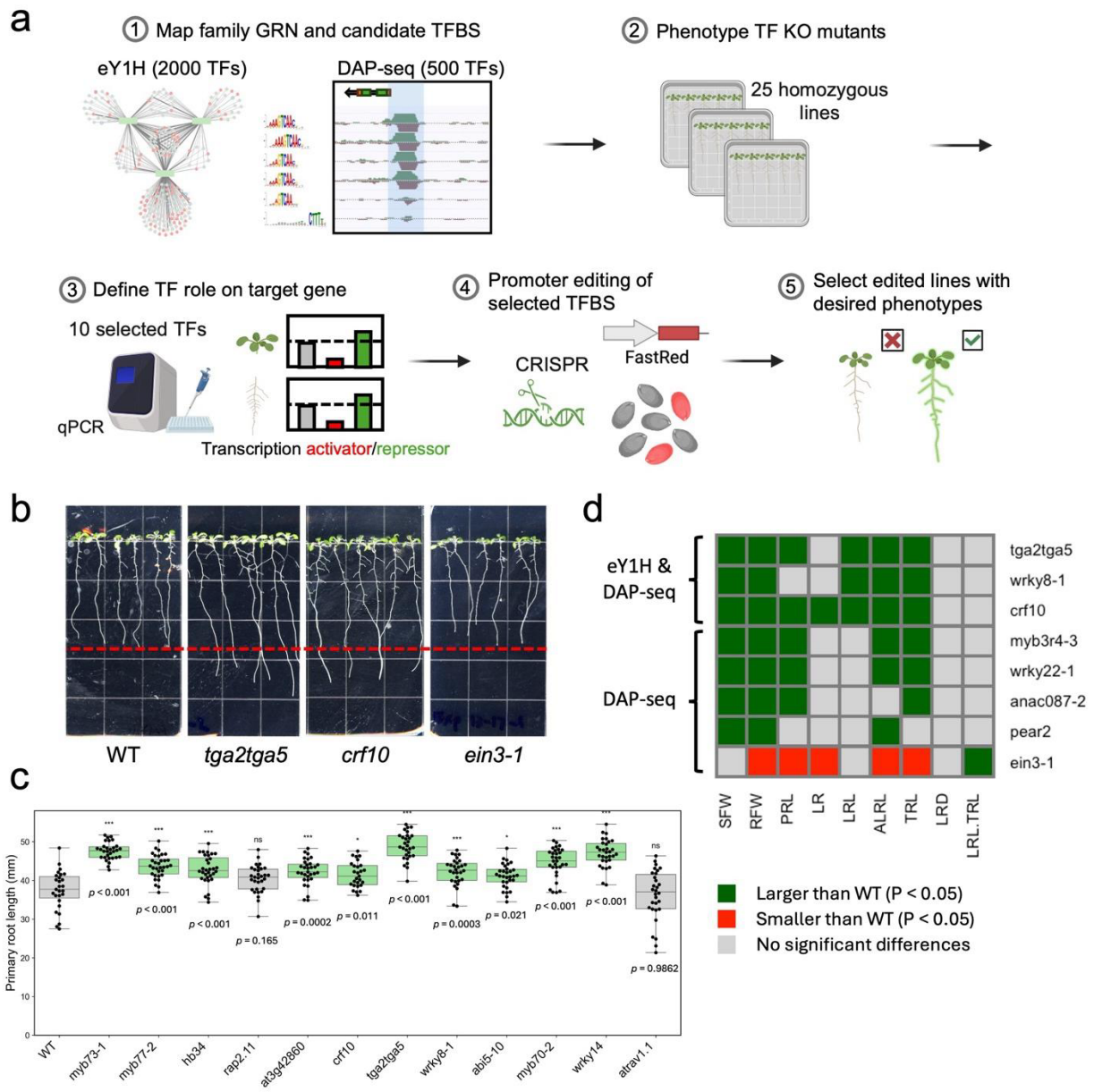

Fig. 2. Identification of putative TFBS.

a. Schematic of the screening and editing workflow applied to *PSY/PSYR* promoters. **b.** Representative 10-day-old TF knockout seedlings identified based on validated TF-promoter interactions. WT, Col-0. **c.** Primary root length of 12 TF knockout mutants at 10 days old. Primary root length of 12 TF knockout mutants at 10 days old. At least 20 plants per genotype were analyzed in each experiment, and the experiment was independently repeated three times. Green indicates a statistically significant increase relative to WT, and grey indicates not significantly different (*** $P < 0.001$, ** $P < 0.01$, * $P < 0.05$, one-way ANOVA; exact n is in Supplementary Data 3).

595 **d.** Heatmap showing phenotypes associated with TF knockout alleles. Selected mutant
596 alleles, identified from both eY1H and DAP-seq or from DAP-seq only, are listed in
597 rows, and measured traits are shown in columns. Statistically significant differences
598 relative to WT are indicated by colored cells ($P < 0.05$, one-way ANOVA; exact n and P
599 values are in Supplementary Data 3). From left to right, traits include shoot fresh weight
600 (SFW, g per 10 seedlings), root fresh weight (RFW, g per 10 seedlings), primary root
601 length (PRL, mm), number of lateral roots (LR), total lateral root length (LRL, mm), total
602 root length (TRL, PRL + LRL, mm), average lateral root length (ALRL, LRL/LR, mm),
603 lateral root density (LRD, LR/PRL), and proportion of total root length contributed by
604 lateral roots (LRL/TRL). Root traits were measured from 10-day-old seedlings. Green
605 indicates a statistically significant increase relative to WT, red indicates a statistically
606 significant decrease, and grey indicates not significantly different from WT ($P < 0.05$,
607 one-way ANOVA; exact n and P values are in Supplementary Data 3).

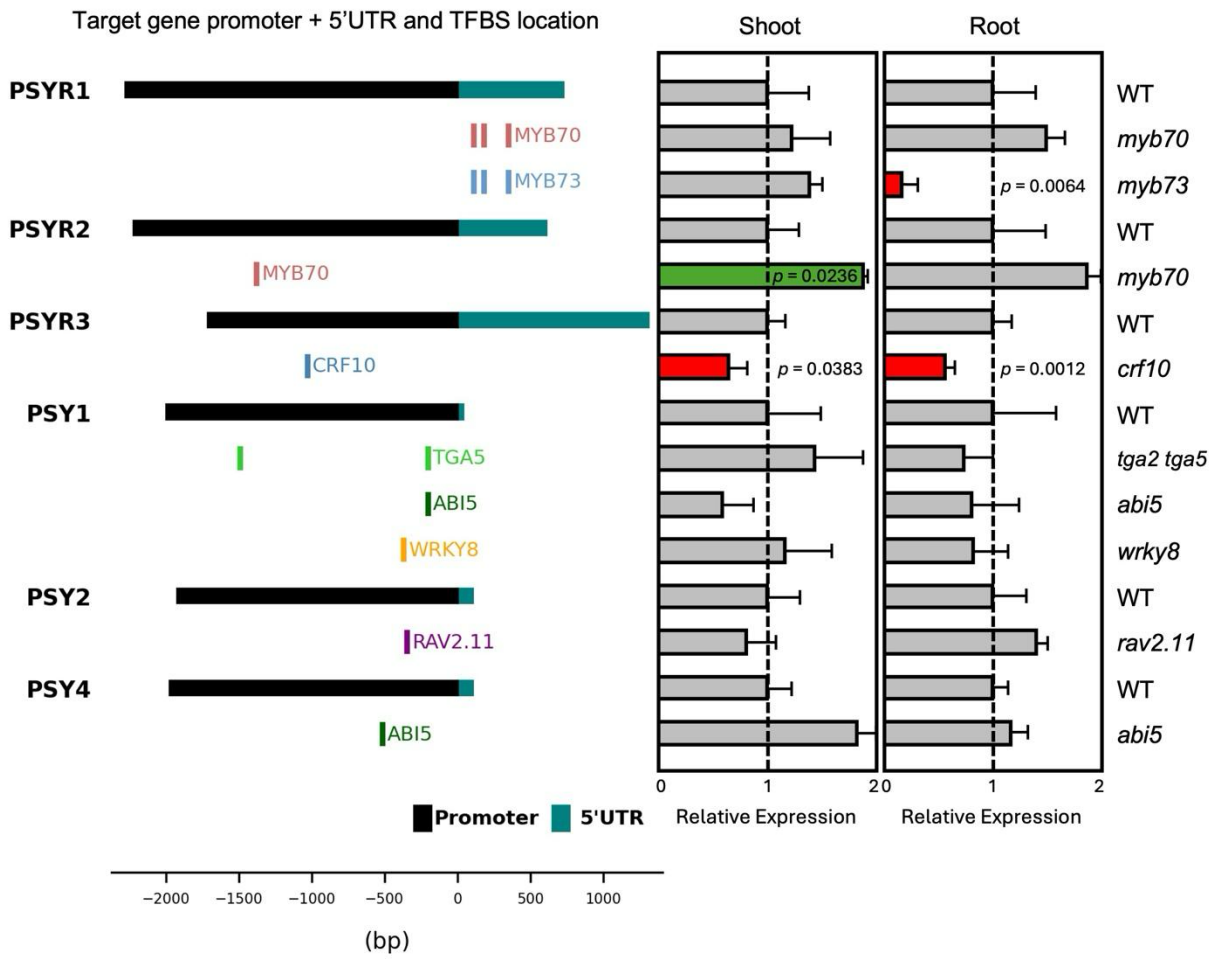

Fig. 3. Organ-specific transcriptional changes in TF knockout mutants.

Expression of targeted *PSY/PSYR* genes in seedling shoots and roots of 10-day-old TF knockout seedlings. Left, schematic of target *PSY/PSYR* promoters and 5'UTR showing the locations of transcription factor binding sites (TFBS) validated via DAP-seq. Right, relative expression of targeted *PSY/PSYR* genes in TF knockout seedlings. For each biological replicate, 10 shoots or 20 roots were pooled. Gene expression was measured by qRT-PCR, with WT normalized to 1 (grey bars). Expression levels significantly increased or decreased in the TF knockout relative to WT are indicated in green (TF is a transcriptional repressor) or red (TF is a transcriptional activator), respectively. Values represent mean ± SD (n = 3 biological replicates).

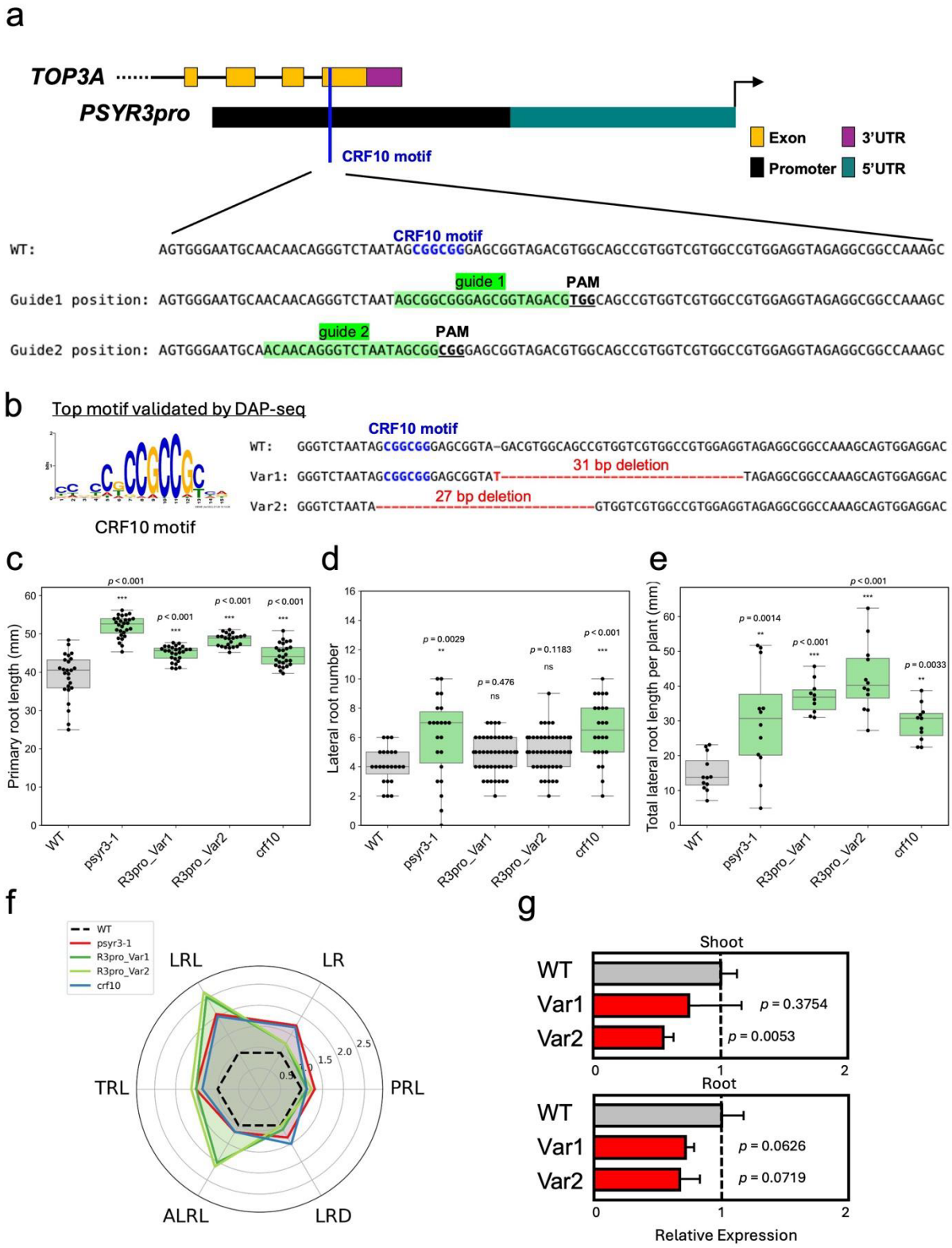

Fig. 4. CRF10 motif editing in the *PSYR3* promoter and the *TOP3A* last exon.

623 **a.** Schematic of the *PSYR3* promoter and *TOP3A* 3' exons showing the CRF10 motif
624 targeted for deletion.
625 **b.** DNA sequence comparison of two promoter-edited variants (Var1 and Var2) relative
626 to WT. Deleted CRF10 motifs are highlighted in red; dashes indicate deleted
627 nucleotides.

628 **c-f.** Root traits measured in 10-day-old seedlings. At least 20 plants per genotype were
629 analyzed in each experiment, and the experiment was independently repeated three
630 times. Green indicates a statistically significant increase relative to WT, and grey
631 indicates not significantly different (*** $P < 0.001$, ** $P < 0.01$, * $P < 0.05$, one-way
632 ANOVA; exact n is in Supplementary Data 3).
633 **c.** Primary root length of WT, *psyr3-1*, *crf10*, and promoter-edited plants. Boxplots show
634 median, interquartile range, and full range.
635 **d.** Number of visible lateral roots per genotype.
636 **e.** Total lateral root length per genotype.
637 **f.** Radar plot comparing root traits across genotypes: PRL, primary root length (mm);
638 LR, number of lateral roots; LRL, total lateral root length (mm); ALRL, average lateral
639 root length (LRL/LR, mm); TRL, total root length (PRL + LRL, mm); LRD, lateral root
640 density (LR/PRL).
641 **g.** *PSYR3* expression in shoot and root organs of 10-day-old promoter-edited seedlings.
642 Values represent mean ± SD (n = 3 biological replicates).
643

644

645 **Supplemental Materials**

646 All supplemental materials referenced in the text will be provided in the final published
647 version. All main findings are fully presented in the figures included in this manuscript.

648

649 **Supplementary Figures**

650

651 **Supplementary Fig. 1. Overlap of eY1H and DAP-seq interactions.**
652 Venn diagram showing TFs identified by either eY1H or DAP-seq for three *PSYR*
653 promoters and nine *PSY* promoters. Yellow circle indicates TFs identified by eY1H, and
654 blue circle indicates TFs identified by DAP-seq.

655 **Supplementary Fig. 2. *PSY/PSYR* expression at the whole plant level.**
656 Data were extracted from the publicly available Arabidopsis RNA-seq (ARS) database
657 (http://ipf.sustech.edu.cn/pub/athrna/).

Supplementary Fig. 3. *PSY/PSYR* expression at the single-cell level in roots.
Data were extracted from the Plant sc-Atlas database.

Supplementary Fig. 4. Expression patterns of candidate TFs identified by both eY1H and DAP-seq.
Data were extracted from the publicly available bulk RNA-seq database.

Supplementary Fig. 5. Confirmation of selected TF knockouts.
qRT-PCR analysis of selected TF expression in TF knockout (KO) mutants. Gene expression was measured by qRT-PCR and normalized to wild-type (WT = 1, grey bars). Expression levels showing a significant decrease are indicated in red. Values represent mean ± SD (n = 3 biological replicates).

Supplementary Fig. 6. Comparison of primary root length in selected Arabidopsis mutant alleles of transcription factors identified by DAP-seq.
Primary root length of 10 TF KO mutants at 10 days old. Exact *P* values are reported in Supplementary Data 3.

Supplementary Fig. 7. CRF10 acts as a negative regulator of plant growth.
a. PCR genotyping confirming the presence of the *GFP-CRF10* transgene.
b. Overexpression of *CRF10* causes an extreme dwarf phenotype. Forty-day-old plants expressing GFP-CRF10 and their segregating wild-type siblings are shown. Scale bar = 1 cm.

Supplementary Datasets

Supplementary Dataset 1. List of eY1H results.

Supplementary Dataset 2. Overlap of eY1H and DAP-seq interactions.

Supplementary Dataset 3. RSA (root system architecture) phenotyping data.

Supplementary Dataset 4. qRT-PCR gene expression data.

Supplementary Tables

Supplementary Table 1. Genotyping, qRT-PCR, and cloning primers.

Supplementary Table 2. Summary of mutants, transgenic plants, and promoter-edited plants.